

PCCP

Accepted Manuscript



This is an *Accepted Manuscript*, which has been through the Royal Society of Chemistry peer review process and has been accepted for publication.

Accepted Manuscripts are published online shortly after acceptance, before technical editing, formatting and proof reading. Using this free service, authors can make their results available to the community, in citable form, before we publish the edited article. We will replace this *Accepted Manuscript* with the edited and formatted *Advance Article* as soon as it is available.

You can find more information about *Accepted Manuscripts* in the [Information for Authors](#).

Please note that technical editing may introduce minor changes to the text and/or graphics, which may alter content. The journal's standard [Terms & Conditions](#) and the [Ethical guidelines](#) still apply. In no event shall the Royal Society of Chemistry be held responsible for any errors or omissions in this *Accepted Manuscript* or any consequences arising from the use of any information it contains.



Journal Name

ARTICLE

Spectroscopic investigation into the design of solid-acid catalysts for the low temperature dehydration of ethanol

Matthew E. Potter,^{a*} Sivan V. Aswegen,^b Emma K. Gibson,^c Ian P. Silverwood^{c,d} and Robert Raja^{b*}

Received 00th January 20xx,
Accepted 00th January 20xx

DOI: 10.1039/x0xx00000x

www.rsc.org/

The increased demand for bulk hydrocarbons necessitates research into increasingly sustainable, energy-efficient catalytic processes. Owing to intricately designed structure-property correlations, SAPO-34 has become established as a promising material for the low temperature ethanol dehydration to produce ethylene. However, further optimization of this process requires a precise knowledge of the reaction mechanism at a molecular level. In order to achieve this a range of spectroscopic characterization techniques are required to probe both the interaction with the active site, and also the wider role of the framework. To this end we employ a combination of in situ infra-red and neutron scattering techniques to elucidate the influence of the surface ethoxy species in the activation of both diethyl ether and ethanol, towards the improved formation of ethylene at low temperatures. The combined conclusions of these studies is that the formation of ethylene is the rate determining step, which is of fundamental importance towards the development of this process and the introduction of bio-ethanol as a viable feedstock for ethylene production.

Introduction

The expanding global population places increased strain on the chemical industry to meet growing demands for bulk and fine chemicals alike.^[1] An example of this is the increased need for ethylene, a major precursor for the pharmaceutical and polymer industries. Currently ethylene is produced from steam cracking of fossil fuels, requiring temperatures exceeding 700 °C.^[2] However, finite reserves of fossil fuels or shale gas cannot solely sustain such growth indefinitely,^[3] inspiring the search for novel precursors. In contrast, biomass-based precursors are considered viable long term options, with bio-ethanol, fermented from sugars, being considered as an alternative feedstock in ethylene production (Figure 1).^[4] This has spurred many to investigate the acid-catalyzed ethanol dehydration as a potential industrial process.^[5-7]

Heterogeneous catalysts have primarily been investigated for ethanol dehydration, as their recyclability and stability is attractive from processing standpoint. Zeotype materials have

been implemented industrially for similar reactions.^[8,9] The ability to confine active-sites within a microporous framework garners great control over the reactants accessing the active site, the intermediary species formed, and the products leaving the active site. Aluminophosphates (AIPOs) have analogous framework topologies as zeolites, though instead of being constructed from corner-sharing SiO₄ tetrahedra, AIPOs are formed from alternating AlO₄ and PO₄ tetrahedra connected by Al-O-P bonds. The ionic nature of the AIPO framework allows the Al³⁺ and P⁵⁺ ions to be isomorphously substituted for a heteroatom, generating a range of active sites.^[8,10-12] Purposeful combinations of a microporous framework with specific dopants, can then lead to the targeted formation of precisely engineered active sites. The most common dopant in AIPOs is silicon (to create a silicon-doped AIPO; SAPO), which leads to the generation of a Brønsted acid site within the framework (Figure S1).^[13] This design approach has been used to great effect in the methanol-to-olefin (MTO) process where SAPO-34 (SAPO with chabazite topology) has been used as a commercial catalyst to produce 3.2 million metric tonnes of propylene and ethylene per year.^[14]

We have recently shown that the isolated Brønsted acid sites within SAPO-34 are active for the ethanol dehydration reaction, achieving ethylene yields of 70% at temperatures as low as 250 °C.^[15] The nature of the active site and the morphology of the framework, have already been studied at great length with a variety of physico-chemical techniques. However, an intricate knowledge of the catalyst in isolation cannot fully account for the distinct interactions and structure-property relationships that occur under reaction conditions in the ethanol dehydration process. Such knowledge requires *in situ* spectroscopic techniques, to identify the intermediate

^a Department of Chemical and Biomolecular Engineering, Georgia Institute of Technology, 311 Ferst Drive, Atlanta, GA 30318, USA.

^b School of Chemistry, University of Southampton, University Road, Southampton, SO17 1BJ, United Kingdom.

^c UK Catalysis Hub, Research Complex at Harwell, Science and Technology Facilities Council Rutherford Appleton Laboratory, Harwell Science and Innovation Campus, Oxon OX11 0QX, United Kingdom.

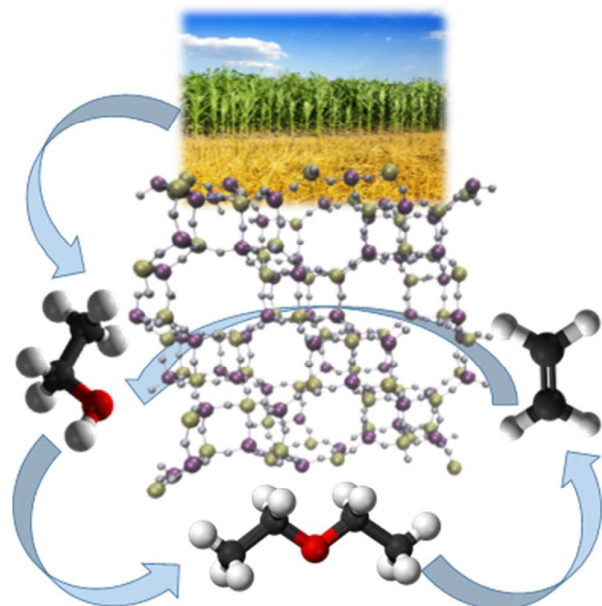
^d ISIS Pulsed Neutron and Muon Facility, Science and Technology Facilities Council Rutherford Appleton Laboratory, Harwell Science and Innovation Campus, Oxon OX11 0QX, United Kingdom.

† Footnotes relating to the title and/or authors should appear here.

Electronic Supplementary Information (ESI) available: [details of any supplementary information available should be included here]. See DOI: 10.1039/x0xx00000x

species formed, and directly observe the behaviour of the reagents and products in the system.^[16,17] To date, a detailed

optimization of a sustainable catalytic process for the low temperature ethanol dehydration to ethylene.



reaction mechanism of

Figure 1: Graphical representation of the SAPO-34 chabazite framework (silver: oxygen, purple: phosphorus, bronze: aluminium), and its use in a possible process to form ethylene from bioethanol, via diethyl ether.

ethanol dehydration in SAPO-34 is unknown. It is widely accepted that diethyl ether is associated with the dehydration reaction, but its precise role as the intermediate or by-product is unclear. It is therefore important to understand the role of diethyl ether, the broader reaction mechanism and the role of the active site, to aid the design and optimization of future processes.

It is emphasized, though often overlooked, that while active-site interactions play a pivotal role in the catalytic process, the separate role of the framework is also highly consequential. The diffusive motion of molecules within the framework often dictates the kinetics and reaction pathway that occur.^[18] However this is often difficult to observe given the limited array of techniques that can provide this information. One such technique is quasi-elastic neutron scattering (QENS). QENS uses incoherent neutron scattering, which is typically dominated by the contributions from hydrogen atoms. This makes it a powerful tool for observing the diffusion of hydrocarbons within a porous inorganic support, as the contribution from the inorganic framework is effectively silenced due to the overwhelming contribution from the hydrocarbon.^[19] This technique has previously synergized well with other *in situ* characterization tools to better understand many catalytic processes.^[20] We therefore present, for the first time, a combined *in situ* FTIR and QENS study on SAPO-34. We aim to integrate knowledge of the specific interactions of the reaction mechanism, with understanding of the structure-property relationships, which dictate the diffusive motion of the organic moieties. This information will facilitate the

Results and discussions

In situ FTIR of ethanol dehydration on SAPO-34

In our previous work^[11,15] we have been able to show how targeted active sites can be formed within SAPO-34. Here silicon was isomorphously substituted into the framework for P (via a type II substitution mechanism, Figure S1), generating strong, isolated Brønsted acid sites.^[15] We were able to show that such systems were capable of producing significant quantities of ethylene at temperatures as low as 250 °C. Here we have replicated the synthesis procedures to create identical, crystalline phase-pure SAPO-34 material (Figure S2) with identical active sites for both FTIR and QENS experiments. In order to make meaningful comparisons the infra-red spectra of the pre-treated SAPO-34 must be considered (Figure 2). The sample was initially heated to 200 °C under a flow of helium, within a DRIFTS cell and then cooled down to 25 °C to remove any previously adsorbed species. On cooling the spectra is typical of SAPO-34 with adsorbed water, showing the interactions between the bridged Brønsted acid hydroxyl species and the physisorbed water.^[21] The presence of the broad $\nu(\text{OH})$ bands at 3678, 3570 and 3500 cm^{-1} , and the absence of the sharp $\nu(\text{OH})$ bands around 3636 and 3599 cm^{-1} confirm that the Brønsted acid sites have been saturated.^[21] This is further evidenced by the broad features at 2890 cm^{-1} and 2475 cm^{-1} , corresponding to water hydrogen bonded with the hydroxyl species.^[21] The other observed region (1500 – 1000 cm^{-1}) is also consistent with physisorbed water, with a broad feature between 1300 and 1200 cm^{-1} due to the bending, $\delta(\text{HOH})$ modes. Other more subtle features are present in this region, including the $\nu(\text{P-O})$ stretch at 1270 cm^{-1} , which is omnipresent in AlPO materials.^[22] Introducing ethanol into the system significantly changes the spectra (Figures 3 and 4). Focusing first on the hydrogen stretching region (4000 to 3000 cm^{-1}) water is displaced by ethanol, as the characteristic broad hydrogen-bonding bands between 3700 – 3500 cm^{-1} are now absent. However, a weak broad feature was observed in the 3200 – 3050 cm^{-1} region (not shown). This represents a peak shift of roughly 400 cm^{-1} for the SAPO-34

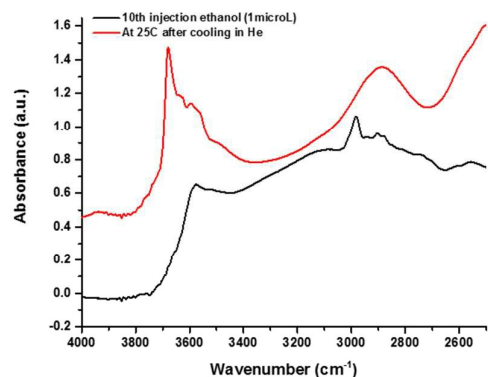


Figure 2: DRIFTS spectra of the SAPO-34 catalyst after pretreatment and cooled to 25 °C (red) contrasted with the DRIFT spectra at 25 °C of the system after the 10th injection of ethanol (1 ul total). The background was recorded using KBr.

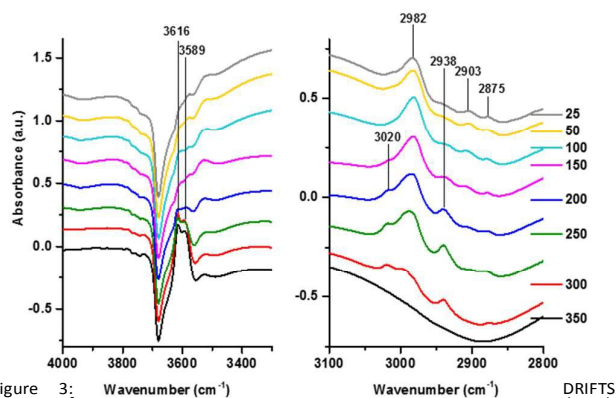


Figure 3: DRIFTS spectra of ethanol-dosed SAPO-34 after a range of temperatures in the O-H and C-H stretching region (4000 – 2500 cm⁻¹). Spectra are presented after subtraction of the spectrum recorded at 25 °C before ethanol injections.

Brønsted acid site, in line with previous reports for the $\Delta\nu(\text{SiOH})$ values for ethanol adsorbed on ZSM-5.^[23] The breadth of the feature indicates that a range of hydrogen-bonded species with multiple configurations and geometries are present. As further evidence that ethanol has displaced water, a range of C-H stretching signals are now present between 3000 and 2870 cm⁻¹.^[23-27] The first two features (2982 and 2938 cm⁻¹) are ascribed to asymmetric stretches of the CH₃ and CH₂ species respectively, whereas the latter two signals (2903 and 2875 cm⁻¹) are the corresponding symmetric stretches.^[24] These species are diagnostic of ethanol interactions with Brønsted acid sites, and have been observed for a range of solid-acid materials, confirming the interactions between ethanol and the SAPO-34 catalyst. In the 1500 to 1000 cm⁻¹ region a range of new features can now be seen, Figure 4. The primary features are strong bands at 1262, 1219 and 1030 cm⁻¹, which are attributed to a mixture of weakly-bound and chemisorbed ethanol species on the SAPO-34 catalyst.^[28]

Increasing the temperature of the system lowers the intensity for the signals attributed to the weakly-bound ethanol species (Figures 3 and 4). The spectra begin to resemble that of purely chemisorbed ethoxy species formed from the reaction of ethanol and Brønsted acid sites to remove water. The broad feature in the O-H stretching region diminishes, and

disappears at 150 °C, confirming that this due to a weakly-bound ethanol species. This is accompanied by a change in the 3000 to 2880 cm⁻¹ region where the intensity of the peaks at 2903 and 2875 cm⁻¹ decrease as the signal at 2938 cm⁻¹ increases.^[24,29] As these signals are still present above 200 °C, they are attributed to the chemisorbed ethoxy species. This is likely due to a decrease in all four of the ethanol peaks (2982, 2938, 2903 and 2875 cm⁻¹), and an increase in the ethoxy signal (2938 and 2982 cm⁻¹). Given the similarity in the species, the position of the bands coincide resulting in a transition from the ethanol signals to the ethoxy signals. Further evidence supporting this theory can be seen in the 1230 region and the 1030 cm⁻¹ band, which rapidly decrease as temperature increases, showing that physisorbed ethanol was also contributing to these bands.^[24,28] Given that the surface ethoxy species and weakly bound ethanol have very similar bands, the exact contributions of the two cannot be distinguished in the C-H or C-C region. However as the temperature increases it is clear the chemisorbed surface ethoxy species become more prevalent in the spectra. Further evidence of the presence of the ethoxy species can be seen at 1485, 1450 and 1395 cm⁻¹.^[28,29] These three signals are characteristic of the surface bound ethoxy species confirming its formation at low temperatures (< 150 °C).^[29] This last observation suggests that the formation of the ethoxy intermediate is energetically favourable in the SAPO-34 system, accounting for the enhanced activity of SAPO-34.

Aside from the ethoxy intermediate, other reaction products can be seen. A subtle feature at 1145 cm⁻¹ is observed, which is commonly attributed to methyl rocking of C-C-O-C-C species, which suggests the early (low temperature) formation of diethyl ether species.^[24,25,30] It is noted that other bands may also be attributed to diethyl ether, though these bands (2982, 2875, 1485, 1450 and 1395 cm⁻¹) typically overlap with ethanol and the ethoxy species.^[24,25,30] The appearance of diethyl ether at low temperature is partly attributed to the strong acid sites present on SAPO-34, and also due to the energetic incentive of forming diethyl ether (-42 kJ/mol). The feature at 1145 cm⁻¹ diminishes, disappearing above 200 °C, coinciding with the appearance of ethylene in the gas-phase mass spectrometry analysis (Figure S3). The disappearance of this band is also accompanied by the broadening of the band at 2880 cm⁻¹. This signal has previously been observed when adsorbing ethylene onto ZSM-5,^[29] suggesting that, at temperatures as low as 200 °C, ethylene is being formed at the acid sites.

It is clear that the initial formation of the ethoxy species is an incredibly fast reaction even at room temperature. As this species survives at reaction temperatures (200 to 300 °C) and only diminishes whilst ethylene is being produced, then it is highly likely to be an active intermediate for this reaction. However, previous literature studies highlight the significant energy barrier required to form ethylene directly from this species,^[31] making it more feasible that this species is able to undergo nucleophilic substitution with an ethanol molecule, to liberate the diethyl ether. The water molecule formed as a result (the energetic driving force of this reaction) then reforms

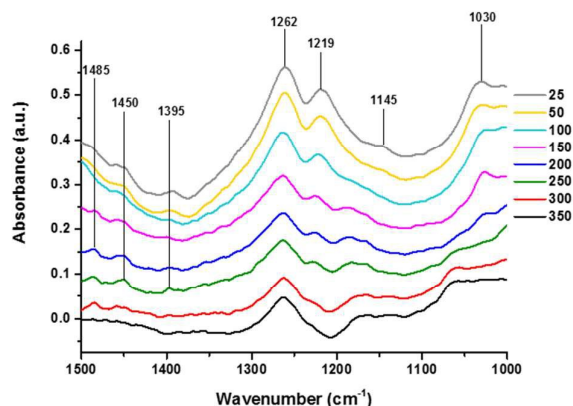


Figure 4: DRIFTS spectra of ethanol-dosed SAPO-34 after a range of temperatures in the O-H and C-H bending region ($1500 - 1000 \text{ cm}^{-1}$). Spectra are presented after subtraction of the spectrum recorded at 25°C before ethanol injections.

the Brønsted acid site. It should be noted that gas-phase ethylene is not observed in the system, given the absence of a broad signal at 3200 cm^{-1} ,^[29] suggesting that that once formed, the ethylene is rapidly desorbed from the system, in agreement with the mass spectrometry data.

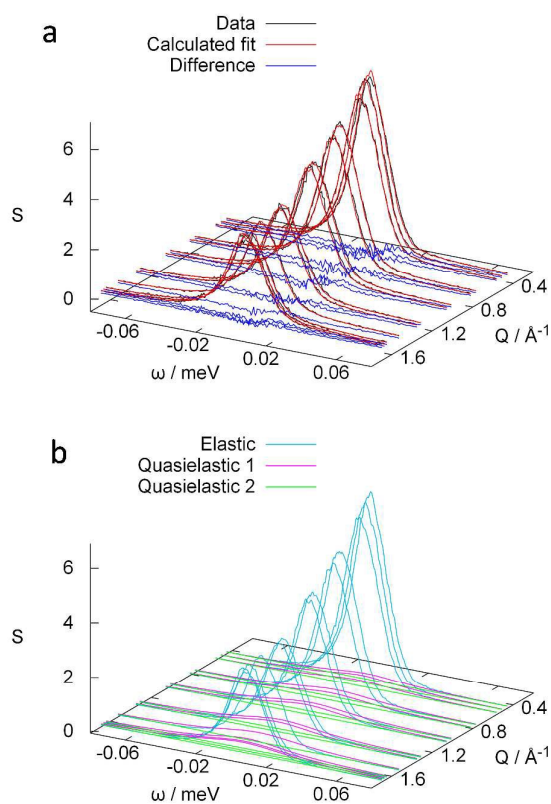
Above 300°C very few features attributed to carbon or hydrogen remain. Among the most resolute species are the ethoxy signals, and also a signal at 3020 cm^{-1} (Figure 3) attributed to olefinic carbon.^[24] Beyond 300°C no organic features remain, showing complete desorption, with the spectra becoming dominated by features attributed to dehydrated SAPO-34. This is evidenced by a pairing of sharp peaks at 3616 and 3589 cm^{-1} (Figure 3) attributed to bridged hydroxyl species with strong Brønsted acidity residing within different locations of the microporous SAPO-34 architecture.^[15] These findings show that the readily formed ethoxy species is a vital intermediate in both the activation of ethanol and towards forming ethylene. In the above spectra we see evidence of ether formation, before ethylene is detected, in either the mass spectrometry or FTIR spectra, suggesting that the rate-determining step of the ethylene formation is the dehydration of ether. To investigate this finding further a quasi-elastic neutron scattering (QENS) study was utilized to probe the relative rates at which the ether and ethanol form the ethoxy species. This would also help to investigate the role of the chabazitic SAPO-34 framework in this process.

Quasi-elastic neutron scattering of ethanol and ether

The crystalline nature of the SAPO-34 framework produces strong coherent elastic scattering signals at specific angles (Bragg peaks) in the QENS spectra. Detectors showing significant coherent scattering were discounted from the analysis, to ensure that the signal recorded was predominantly incoherent, therefore selectively focusing on the motion of the hydrocarbon species, for effective QENS analysis (Figure S4). The SAPO-34 catalyst was separated into two batches, one loaded with ether and the other with ethanol, introduced through a helium bubbler. To probe variation with

temperature in both sorbates, spectra were taken at 25 , 50 , 75 , 100 and 125°C .

The initial spectra of ethanol-loaded SAPO-34 at 25°C (Figure 5) was fitted using the convolution of a measured resolution function with one elastic component (δ) and two quasi-elastic components; a narrower Lorentzian (L1) and a broader Lorentzian (L2), corresponding to two different modes of motion within the system. Plotting the FWHM of the Lorentzian signals vs Q^2 showed that L1 varies at low Q , before plateauing at higher Q . This behaviour is symptomatic of jump diffusion within a confined area, such as within a pore.^[32-34] This confirms that ethanol is able to penetrate the micropores of the SAPO-34 species, and access the internal acid sites of the catalyst, though does not diffuse in a smooth continuous fashion. The broader Lorentzian (L2) seems invariant of Q , suggesting rotational motion. As ethanol is able to penetrate the pores it is unlikely this is due to pore-blockage. Instead this



is attributed to a strong

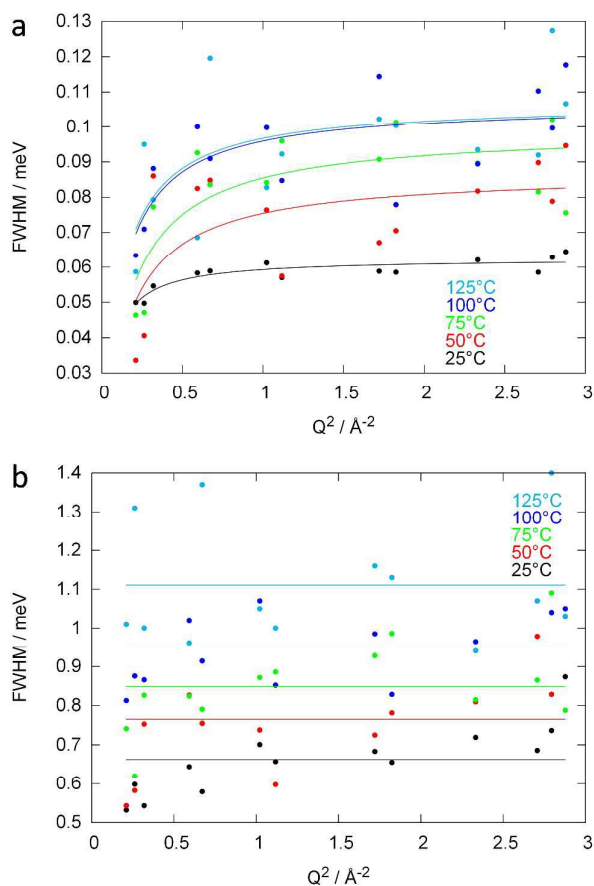
Figure 5: QENS spectra of SAPO-34 loaded with ethanol at 25°C , comparing the fitted and experimental data (a) and showing the individual components (b).

interaction between the Brønsted acid species and the ethanol, anchoring the ethanol to the pore wall, thereby hindering diffusion. Given the findings in the FTIR data this is attributed to the readily formed surface ethoxy species. As such quasi-elastic components attributed to 'free' ethanol and 'bound' ethoxy species can be readily discerned from the data. As the temperature is increased both Lorentzian components broaden (Figures 6 and S5-S8), becoming more intense relative

to the elastic component. Plotting the FWHM of the narrower L1 component against Q^2 for the different temperatures revealed a common shape, showing that the nature of the motion did not change with temperature. However, as expected the gradient of the curve became steeper at lower Q , and the limits reached at high Q values increased. Both observations are consistent with increased diffusivity at higher temperatures, as expected. Fitting this data to a Singwi Sjolander jump diffusion model^[35] showed that as the temperature increased the residence time of the ethanol molecules decreased (Table 1), and the mean square displacement increased. The diffusion constants of this process were calculated from the parameters obtained using $D = \langle r^2 \rangle / 6\tau$, and was found to increase with temperature. Arrhenius plots of this data found the activation energy for this process to be 9 kJ/mol which is in the range expected for a small molecule in a confined space (Figure 7).^[36-38] The data point at 298 K does not fit this trend, we attribute this to the

motion (L2) was also found to increase with temperature, however remained invariant with Q , indicating rotational motion. Similar Arrhenius analysis of this function showed that the activation energy for rotation was 5 kJ/mol (Figure S9), again in line with previous studies.^[36-38]

The elastic incoherent scattering function (EISF) allows the intensity of the individual quasi-elastic components to be compared with the elastic component (Figure 8). The EISF for the component corresponding to jump diffusion of free ethanol (Figure 8a), decreases at higher temperatures, showing an increase in the relative intensity of this component with respect to the elastic component. This shows that there is increased motion with increasing temperature. The shape of the EISF shows an approximately linear decrease, preventing further quantitative analysis, as such is not readily fit to a common model. The EISF for the rotational motion of bound ethoxy species (Figure 8b) is a similar shape to the jump diffusion component, however greater variance with temperature is seen. These findings in combination with the FTIR show that ethanol forms significant quantities of the ethoxy species, even



formation of the surface ethoxy species at room

Figure 6: The influence of temperature on the relationship between the narrow Lorentzian (L1, a) which is fitted to a Singwi Sjolander jump model, and the broad Lorentzian (L2, b) that is fit as a constant value for the ethanol-loaded SAPO-34 system.

temperature, making the Singwi Sjolander model inappropriate at this temperature, as such it was excluded from the Arrhenius calculation. The FWHM for the rotational

Table 1: Derived parameters from the models fitting the ethanol-loaded QENS SAPO-34 data.

Temp/°C	L1, Singwi Sjolander			L2, Rotation	
	τ/ps	$\langle r^2 \rangle / \text{Å}^2$	$D/(\text{m}^2\text{s}^{-1})$	τ/ps	$D/(\text{s}^{-1})$
25	21.3	110.0	8.60×10^{-9}	2.01	4.98×10^{11}
50	15.3	39.4	4.29×10^{-9}	1.74	5.75×10^{11}
75	13.4	37.4	4.65×10^{-9}	1.57	6.38×10^{11}
100	12.5	53.4	7.15×10^{-9}	1.40	7.14×10^{11}
125	12.4	55.8	7.49×10^{-9}	1.20	8.35×10^{11}

at a low temperature (see later discussions). There are few signs that the quantity of ethoxy species is changing drastically with temperature. This is likely due to the fact that the ethoxy forms almost instantaneously, saturating the majority of the Brønsted acid sites at low temperatures. This allows the excess ethanol to move freely through the pores. The positive correlation between diffusion constants and temperature for both processes shows that the both the ethoxy and ethanol species are able to move more rapidly in the system as expected.

QENS spectra of SAPO-34 loaded with diethyl ether were also recorded at 25, 50, 75, 100 and 125 °C (Figures S10–S14), and fitted in an analogous fashion with one elastic, and one narrow (L3) and one broad (L4) quasielastic Lorentzian components. Analysis of the FWHM of the Lorentzians as a function of Q^2 (Figure S15) shows that both modes are constant for all Q values. The latter (L4) has a similar range of FWHM and similar shape to the rotational motion observed in ethanol, however the shape of the narrower (L3) Lorentzian means it cannot be assigned based on this one temperature. At higher temperatures the FWHM of L4 increases, however still remains constant with respect to Q^2 (Figure S15b) confirming that this is a rotational motion similar to ethanol. Again the residence time is reduced as temperature increases (Table 2), leading to

an activation energy of 2.2 kJ/mol (Figure 9). In contrast increasing the temperature shows L3 begins to resemble the shape of a confined jump diffusion model (Figure S15a) similar to ethanol,

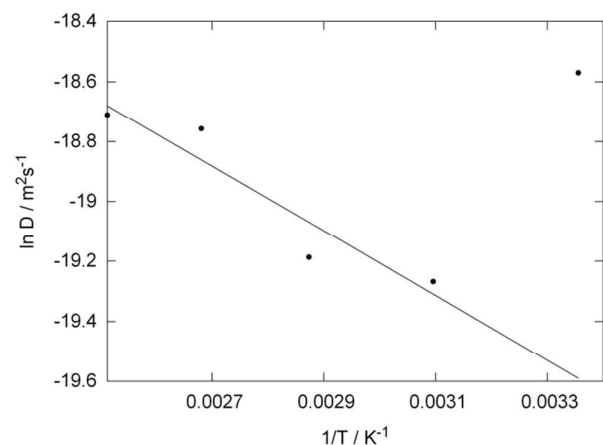


Figure 7: Arrhenius plot of the jump diffusion process (L1) occurring in ethanol-loaded SAPO-34. The diffusion constant decreases with decreasing temperature, resulting in an activation energy of 9 kJ/mol.

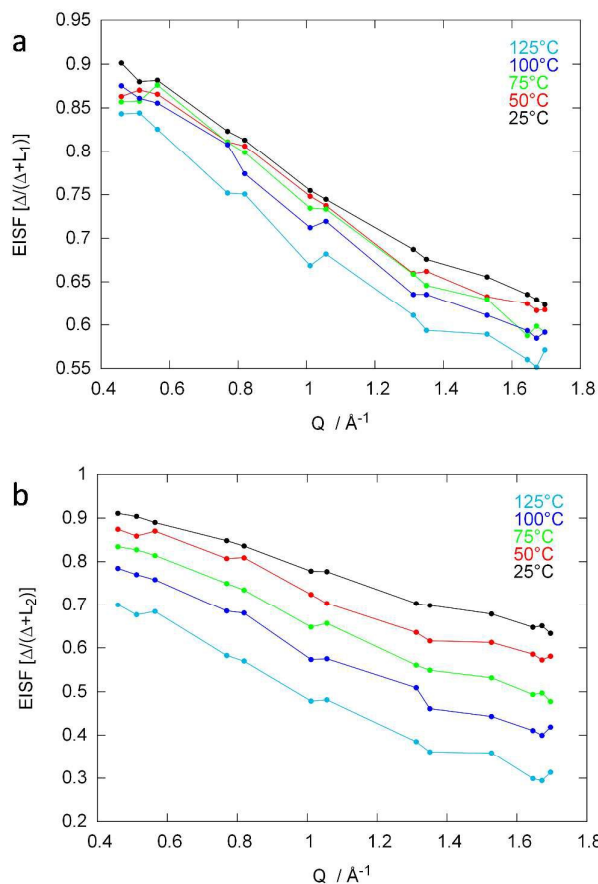


Figure 8: EISF of the individual Lorentzian components of ethanol-loaded SAPO-34, showing decreasing EISF values with temperature and Q for the narrow Lorentzian (L1, a) and the broader Lorentzian (L2, b).

again the FWHM increasing as a function of temperature. This suggests that this is also due to 'free' ether undergoing translational diffusion within the confined SAPO-34 pore, showing that the ether is also able to access the internal sites of SAPO-34. Fitting L3 to a Singwi Sjolander model shows a decrease in the residence time (as expected) but a decrease in $\langle r^2 \rangle$, resulting in the diffusion constant decreasing as a function of temperature is unexpected until one considers the FTIR findings and the thermochemistry of the reaction steps. It has been previously established¹⁵ that ethanol readily forms the bound ethoxy species, which will partially block the pores and hinder diffusion. At room temperature a large proportion of the Brønsted acid sites in SAPO-34 have already formed the ethoxy species. Increasing the temperature will not significantly increase the number of ethoxy species, as such the 'free' ethanol species experience a constant level of pore blockage, and therefore behave as expected when the temperature is increased.¹⁵ Further evidence of this can be seen in the EISF for the ether-loaded SAPO-34, (Figure 10) where the EISF for L3 shows no significant variation with temperature. This is contrary to the ethanol data, though is explained by considering that at

Table 2: Derived parameters from the models fitting the ethanol-loaded QENS

Temp/ $^{\circ}$ C	L1, Singwi Sjolander			L2, Rotation	
	τ /ps	$\langle r^2 \rangle / \text{\AA}^2$	$D / (\text{m}^2 \text{s}^{-1})$	τ /ps	$D / (\text{s}^{-1})$
25	16.0	2.35×10^9	2.45×10^{-2}	1.66	6.02×10^{11}
50	14.5	177	2.03×10^{-8}	1.70	5.88×10^{11}
75	12.8	86	1.12×10^{-8}	1.58	6.33×10^{11}
100	11.4	51	7.46×10^{-9}	1.47	6.80×10^{11}
125	10.4	39	6.25×10^{-9}	1.34	7.46×10^{11}

SAPO-34 data.

higher temperatures the 'free' ether species (that contribute to the L3 component) are becoming 'bound' ethoxy species, and therefore limiting the area of the L3 component relative to the elastic component, confirming that ethanol is more readily activated than ether.¹⁵

These findings emphasize the importance of employing a framework that is appropriately suited for the dehydration of ethanol. The importance of the active site has already been discussed from a purely structural viewpoint, whereby the formation of isolated acid sites exclusively through type II substitution facilitates the formation of stronger Brønsted acid sites. It is now apparent that such active acid sites should be attuned not just for the activation of the ethanol reactant, but also for the diethyl ether intermediate. Further, the framework dimensions play a pivotal role: SAPO-34 is a small-pored zeotype species (3.8 Å pore diameter), therefore the formation of ethoxy species within the pore significantly retards hydrocarbon diffusion through the framework. In doing so, the hydrocarbon species become trapped near active ethoxy species and Brønsted acid sites, increasing the likelihood of favorable interactions that can initiate, or enhance the

catalytic pathway, akin to product selectivity observed in previous catalytic zeotype studies.^[8,39] It has already been shown that the larger pore SAPO-5 species (AFI framework, 7.3 Å pore

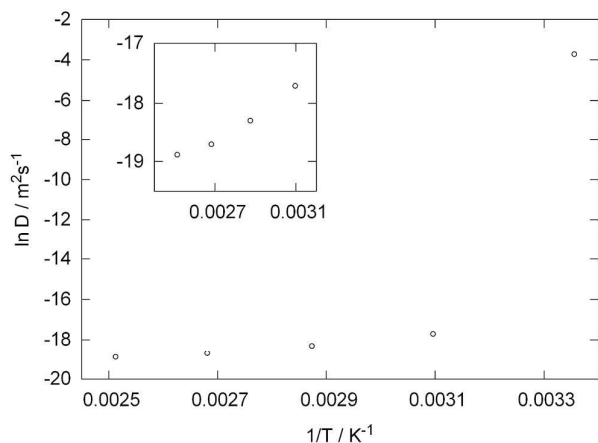


Figure 9: Arrhenius plot of the jump diffusion process (L3) in diethyl-ether loaded SAPO-34. The diffusion constant decreases with increasing temperature.

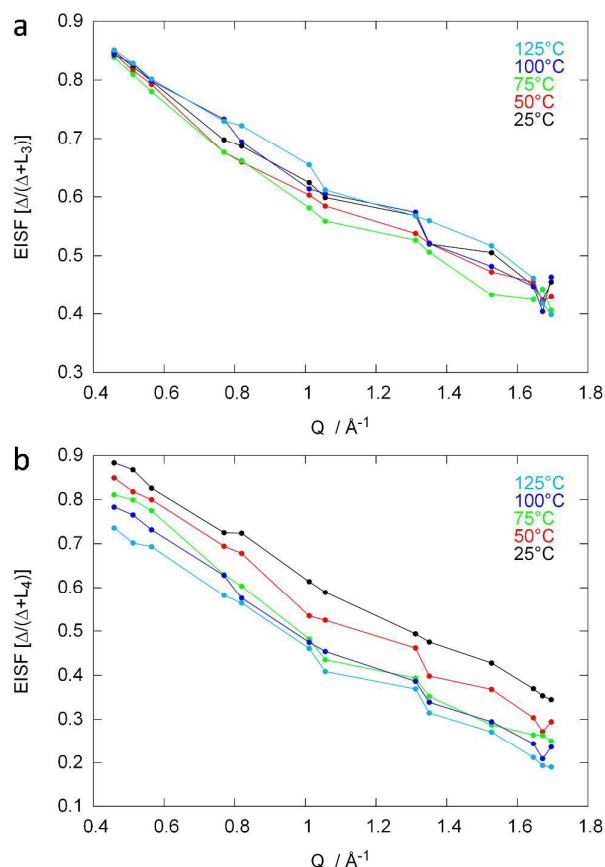


Figure 10: EISF of the individual Lorentzian components of ether-loaded SAPO-34, showing decreasing EISF values with temperature and Q for the narrow Lorentzian (L3, a) and the broader Lorentzian (L4, b).

diameter) is catalytically inferior than the SAPO-34 species,^[15] which was previously attributed to the difference in active sites. It is now clear that the precise framework architecture also plays a vital role, as the larger pores of SAPO-5 would not hinder diffusion to the same extent as SAPO-34, allowing a greater proportion of molecules to pass through the pores without reacting. However the formation of ethoxy species significantly limits the diffusion in the small-pore SAPO-34, enhancing the reactivity of the catalyst towards a greater ethylene yield.

Conclusions

The low temperature catalytic dehydration of ethanol offers attractive potential for the use of biomass derived feedstocks, which can facilitate the more sustainable the production of ethylene. SAPO-34 has previously demonstrated high yields for this process at temperatures as low as 250 °C. Understanding the catalytic reaction at the molecular level offers the possibility for further optimization of the reaction at lower temperatures. Using a combined *in situ* FTIR and QENS study we have been able to directly probe the elementary steps of the acid-catalysed dehydration mechanism. *In situ* FTIR has highlighted the importance of the surface ethoxy species as an intermediate in the reaction. Combining these findings with a QENS study contrasted the behaviour of ethanol and ether loaded SAPO-34 samples, showing that the 'bound' ethoxy species is readily formed from ethanol whereas higher temperatures are required for subsequent ethylene production. This confirms that the rate limiting step in this reaction is the formation of the ethylene, the improvement of which should form the basis of future studies for this system. It is believed that this fundamental knowledge of the reaction mechanism will now enable the augmentation of both catalytic materials and the overall process towards the improved, more selective, production of ethylene at low temperatures.

Acknowledgements

The UK Catalysis Hub is kindly thanked for resources and support provided via our membership of the UK Catalysis Hub Consortium and funded by EPSRC (grants EP/K014706/1, EP/K014668/1, EP/K014854/1EP/K014714/1 and EP/M013219/1), via our membership of the UK's HEC Materials Chemistry Consortium, which is funded by EPSRC (EP/L000202). MEP and SVA would also like to thank Honeywell LLC for their studentship bursary.

Notes and references

- 1 A. Morschbacker, *Polym. Rev.*, 2009, **49**, 79.
- 2 Y. Gucbilmez, T. Dogu and S. Balci, *Ind. Eng. Chem. Res.*, 2006, **45**, 3496.
- 3 P. C. A. Pieter and B. M. Weckhuysen, *Angew. Chem. Int. Ed.*, 2013, **52**, 11980.
- 4 M. Zhang and Y. Yu, *Ind. Eng. Chem. Res.*, 2013, **52**, 9505.

- 5 M. Lefenfeld, R. Raja, A. J. Paterson and M. E. Potter, *US Patent*, 2015, US9012709 B2.
- 6 T. K. Phung and G. Busca, *Catal. Commun.*, 2015, **68**, 110.
- 7 J. Sun and Y. Wang, *ACS Catal.*, 2014, **4**, 1078.
- 8 R. Raja, M. E. Potter and S. H. Newland, *Chem. Commun.*, 2014, **50**, 5940.
- 9 N. Rahimi and R. Karimzadeh, *Appl. Catal. A: Gen.*, 2011, **398**, 1.
- 10 M. E. Potter, A. J. Paterson, B. Mishra, S. D. Kelly, S. R. Bare, F. Cora, A. B. Levy and R. Raja, *J. Am. Chem. Soc.*, 2015, **137**, 8534.
- 11 E. Gianotti, M. Manzoli, M. E. Potter, V. N. Shetti, D. Sun, J. Paterson, T. M. Mezza, A. Levy and R. Raja, *Chem. Sci.*, 2014, **5**, 1810.
- 12 E. Morra, S. Maurelli, M. Chiesa and E. Giamello, *Topics in Catal.*, 2015, **58**, 783.
- 13 C. S. Blackwell and R. L. Patton, *J. Phys. Chem.*, 1988, **92**, 3965.
- 14 <https://www.honeywellprocess.com/en-US/news-and-events/Pages/pr12012015-honeywell-technology-helping-chinese-company-tap-crude-oil-alternatives-to-meet-growing-demand-for-plastics.aspx>
- 15 M. E. Potter, M. E. Cholerton, J. Kezina, R. Bounds, M. Carravetta, M. Manzoli, E. Gianotti, M. Lefenfeld and R. Raja, *ACS Catal.*, 2014, **4**, 4161.
- 16 S. Bordiga, E. Groppo, G. Agostini, J. A. van Bokhoven and C. Lamberti, *Chem. Rev.*, 2013, **113**, 1736.
- 17 B. S. Yeo and A. T. Bell, *J. Phys. Chem. C*, 2012, **116**, 8394.
- 18 H. Jobic, and D. N. Theodorou, *J. Phys. Chem C*, 2006, **110**, 1964.
- 19 H. Jobic and D. N. Theodorou, *Micropor. Mesopor. Mater.*, 2007, **102**, 21.
- 20 A. J. O'Malley, S. F. Parker, A. Chutia, M. R. Farrow, I. P. Silverwood, V. Garcia-Sakai and C. R. A. Catlow, *Chem. Commun.*, 2016, **52**, 2897.
- 21 A. Zecchina, F. Geobaldo, G. Spoto, S. Bordiga, G. Ricchiardi, R. Buzzoni and G. Petrini, *J. Phys. Chem.*, 1996, **100**, 16584.
- 22 M. Rokita, M. Handke and W. Mozgawa, *J. Mol. Struct.*, 2000, **555**, 351.
- 23 A. Zecchina, S. Bordiga, G. Spoto, D. Scarano, G. Spano and F. Geobaldo, *J. Chem. Soc., Faraday Trans.*, 1996, **92**, 4863.
- 24 Z. S. B. Sousa, D. B. Cesar, C. A. Henriques and V. T. da Silva, *Catal. Today*, 2014, **234**, 182.
- 25 P. Li and L. M. Ng, *Surf. Sci.*, 1995, **342**, 359.
- 26 T. K. Phung, A. Lagazzo, M. A. R. Crespo, V. S. Escribano and G. Busca, *J. Catal.*, 2014, **311**, 102.
- 27 K. Hemelsoet, A. Ghysels, D. Mores, K. De Wispelaere, V. Van Speybroeck, B. M. Weckhuysen and M. Waroquier, *Catal. Today*, 2011, **177**, 12.
- 28 T. K. Phung and G. Busca, *Chem. Eng. J.*, 2015, **272**, 92.
- 29 H. Yamazaki, T. Yokoi, T. Tatsumi and J. N. Kondo, *Catal. Sci. Technol.*, 2014, **4**, 4193.
- 30 G. A. M. Hussein, N. Sheppard, M. I. Zaki and R. B. Fahim, *J. Chem. Soc. Faraday Trans.*, 1991, **87**, 2661.
- 31 J. N. Kondo, D. Nishioka, H. Yamazaki, J. Kubota, K. Domen and T. Tatsumi, *J. Phys. Chem. C*, 2010, **114**, 20107.
- 32 P. L. Hall and D. K. Ross, *Mol. Phys.*, 1981, **42**, 673.
- 33 H. Jobic, A. N. Fitch and J. Combet, *J. Phys. Chem. B*, 2000, **104**, 8491.
- 34 H. Paoli, A. Methievier, H. Jobic, C. Krause, H. Pfeifer, F. Stallmach and J. Karger, *Micropor. Mesopor. Mater.*, 2002, **55**, 147.
- 35 K. S. Singwi and A. Sjolander, *Phys. Rev.*, 1960, **120**, 1093.
- 36 H. Jobic, J. Karger, C. Krause, S. Brandani, A. Gunadi, A. Methivier, C. Ehlers, B. Farago, W. Haeussler and D. M. Ruthven, *Adsorp.*, 2005, **11**, 403.
- 37 K. Yoo, R. Tsekov and P. G. Smirniotis, *J. Phys. Chem. B*, 2003, **107**, 13593.
- 38 E. Yoda, J. N. Kondo and K. Domen, *J. Phys. Chem. B*, 2005, **109**, 1464.
- 39 M. Dugal, G. Sankar, R. Raja and J. M. Thomas, *Angew. Chem. Int. Ed.*, 2000, **39**, 2310.